

Multiresolution Gray-Scale and Rotation Invariant Texture Classification with Local Binary Patterns

Timo Ojala, Matti Pietikäinen, *Senior Member, IEEE*, and Topi Mäenpää

Abstract—This paper presents a theoretically very simple, yet efficient, multiresolution approach to gray-scale and rotation invariant texture classification based on local binary patterns and nonparametric discrimination of sample and prototype distributions. The method is based on recognizing that certain local binary patterns, termed “uniform,” are fundamental properties of local image texture and their occurrence histogram is proven to be a very powerful texture feature. We derive a generalized gray-scale and rotation invariant operator presentation that allows for detecting the “uniform” patterns for any quantization of the angular space and for any spatial resolution and presents a method for combining multiple operators for multiresolution analysis. The proposed approach is very robust in terms of gray-scale variations since the operator is, by definition, invariant against any monotonic transformation of the gray scale. Another advantage is computational simplicity as the operator can be realized with a few operations in a small neighborhood and a lookup table. Excellent experimental results obtained in true problems of rotation invariance, where the classifier is trained at one particular rotation angle and tested with samples from other rotation angles, demonstrate that good discrimination can be achieved with the occurrence statistics of simple rotation invariant local binary patterns. These operators characterize the spatial configuration of local image texture and the performance can be further improved by combining them with rotation invariant variance measures that characterize the contrast of local image texture. The joint distributions of these orthogonal measures are shown to be very powerful tools for rotation invariant texture analysis.

Index Terms—Nonparametric, texture analysis, Outex, Brodatz, distribution, histogram, contrast.



1 INTRODUCTION

ANALYSIS of two-dimensional textures has many potential applications, for example, in industrial surface inspection, remote sensing, and biomedical image analysis, but only a limited number of examples of successful exploitation of texture exist. A major problem is that textures in the real world are often not uniform due to variations in orientation, scale, or other visual appearance. The gray-scale invariance is often important due to uneven illumination or great within-class variability. In addition, the degree of computational complexity of most proposed texture measures is too high, as Randen and Husoy [32] concluded in their recent extensive comparative study involving dozens of different spatial filtering methods: “A very useful direction for future research is therefore the development of powerful texture measures that can be extracted and classified with a low-computational complexity.”

Most approaches to texture classification assume, either explicitly or implicitly, that the unknown samples to be classified are identical to the training samples with respect to spatial scale, orientation, and gray-scale properties. However, real-world textures can occur at arbitrary spatial

resolutions and rotations and they may be subjected to varying illumination conditions. This has inspired a collection of studies which generally incorporate invariance with respect to one or at most two of the properties spatial scale, orientation, and gray scale.

The first few approaches on rotation invariant texture description include generalized cooccurrence matrices [12], polarograms [11], and texture anisotropy [7]. Quite often an invariant approach has been developed by modifying a successful noninvariant approach such as MRF (Markov Random Field) model or Gabor filtering. Examples of MRF-based rotation invariant techniques include the CSAR (circular simultaneous autoregressive) model by Kashyap and Khotanzad [16], the MRSAR (multiresolution simultaneous autoregressive) model by Mao and Jain [23], and the works of Chen and Kundu [6], Cohen et al. [9], and Wu and Wei [37]. In the case of feature-based approaches, such as filtering with Gabor wavelets or other basis functions, rotation invariance is realized by computing rotation invariant features from the filtered images or by converting rotation variant features to rotation invariant features [13], [14], [15], [19], [20], [21], [22], [30], [39]. Using a circular neighbor set, Porter and Canagarajah [31] presented rotation invariant generalizations for all three mainstream paradigms: wavelets, GMRF, and Gabor filtering. Utilizing similar circular neighborhoods, Arof and Deravi obtained rotation invariant features with 1D DFT transformation [2].

A number of techniques incorporating invariance with respect to both spatial scale and rotation have been presented [1], [9], [20], [22], [38], [39]. The approach based

• The authors are with the Machine Vision and Media Processing Unit, Infotech Oulu, University of Oulu, PO Box 4500, FIN-90014, Finland.
E-mail: {skidi, mtkp, topiollu}@ee.oulu.fi.

Manuscript received 13 June 2000; revised 21 June 2001; accepted 16 Oct. 2001.

Recommended for acceptance by D. Jacobs.

For information on obtaining reprints of this article, please send e-mail to: tpami@computer.org, and reference IEEECS Log Number 112278.

on Zernike moments by Wang and Healey [36] is one of the first studies to include invariance with respect to all three properties: spatial scale, rotation, and gray scale. In his mid-1990s survey on scale and rotation invariant texture classification, Tan [35] called for more work on perspective projection invariant texture classification, which has received a rather limited amount of attention [5], [8], [17].

This work focuses on gray-scale and rotation invariant texture classification, which has been addressed by Chen and Kundu [6] and Wu and Wei [37]. Both studies approached gray-scale invariance by assuming that the gray-scale transformation is a linear function. This is a somewhat strong simplification, which may limit the usefulness of the proposed methods. Chen and Kundu realized gray-scale invariance by global normalization of the input image using histogram equalization. This is not a general solution, however, as global histogram equalization cannot correct intrimage (local) gray-scale variations.

In this paper, we propose a theoretically and computationally simple approach which is robust in terms of gray-scale variations and which is shown to discriminate a large range of rotated textures efficiently. Extending our earlier work [27], [28], [29], we present a gray-scale and rotation invariant texture operator based on local binary patterns. Starting from the joint distribution of gray values of a circularly symmetric neighbor set of pixels in a local neighborhood, we derive an operator that is, by definition, invariant against any monotonic transformation of the gray scale. Rotation invariance is achieved by recognizing that this gray-scale invariant operator incorporates a fixed set of rotation invariant patterns.

The main contribution of this work lies in recognizing that certain local binary texture patterns termed “uniform” are fundamental properties of local image texture and in developing a generalized gray-scale and rotation invariant operator for detecting these “uniform” patterns. The term “uniform” refers to the uniform appearance of the local binary pattern, i.e., there are a limited number of transitions or discontinuities in the circular presentation of the pattern. These “uniform” patterns provide a vast majority, sometimes over 90 percent, of the 3×3 texture patterns in examined surface textures. The most frequent “uniform” binary patterns correspond to primitive microfeatures, such as edges, corners, and spots; hence, they can be regarded as feature detectors that are triggered by the best matching pattern.

The proposed texture operator allows for detecting “uniform” local binary patterns at circular neighborhoods of any quantization of the angular space and at any spatial resolution. We derive the operator for a general case based on a circularly symmetric neighbor set of P members on a circle of radius R , denoting the operator as $LBP_{P,R}^{riu2}$. Parameter P controls the quantization of the angular space, whereas R determines the spatial resolution of the operator. In addition to evaluating the performance of individual operators of a particular (P, R) , we also propose a straightforward approach for multiresolution analysis, which combines the responses of multiple operators realized with different (P, R) .

The discrete occurrence histogram of the “uniform” patterns (i.e., the responses of the $LBP_{P,R}^{riu2}$ operator)

computed over an image or a region of image is shown to be a very powerful texture feature. By computing the occurrence histogram, we effectively combine structural and statistical approaches: The local binary pattern detects microstructures (e.g., edges, lines, spots, flat areas) whose underlying distribution is estimated by the histogram.

We regard image texture as a two-dimensional phenomenon characterized by two orthogonal properties: spatial structure (pattern) and contrast (the “amount” of local image texture). In terms of gray-scale and rotation invariant texture description, these two are an interesting pair: Where spatial pattern is affected by rotation, contrast is not, and vice versa, where contrast is affected by the gray scale, spatial pattern is not. Consequently, as long as we want to restrict ourselves to pure gray-scale invariant texture analysis, contrast is of no interest as it depends on the gray scale.

The $LBP_{P,R}^{riu2}$ operator is an excellent measure of the spatial structure of local image texture, but it, by definition, discards the other important property of local image texture, i.e., contrast, since it depends on the gray scale. If only rotation invariant texture analysis is desired, i.e., gray-scale invariance is not required, the performance of $LBP_{P,R}^{riu2}$ can be further enhanced by combining it with a rotation invariant variance measure $VAR_{P,R}$ that characterizes the contrast of local image texture. We present the joint distribution of these two complementary operators, $LBP_{P,R}^{riu2}/VAR_{P,R}$, as a powerful tool for rotation invariant texture classification.

As the classification rule, we employ nonparametric discrimination of sample and prototype distributions based on a log-likelihood measure of the dissimilarity of histograms, which frees us from making any, possibly erroneous, assumptions about the feature distributions.

The performance of the proposed approach is demonstrated with two experiments. Excellent results in both experiments demonstrate that the proposed texture operator is able to produce, from just one reference rotation angle, a representation that allows for discriminating a large number of textures at other rotation angles. The operators are also computationally attractive as they can be realized with a few operations in a small neighborhood and a lookup table.

The paper is organized as follows: The derivation of the operators and the classification principle are described in Section 2. Experimental results are presented in Section 3 and Section 4 concludes the paper.

2 GRAY SCALE AND ROTATION INVARIANT LOCAL BINARY PATTERNS

We start the derivation of our gray scale and rotation invariant texture operator by defining texture T in a local neighborhood of a monochrome texture image as the joint distribution of the gray levels of P ($P > 1$) image pixels:

$$T = t(g_c, g_0, \dots, g_{P-1}), \quad (1)$$

where gray value g_c corresponds to the gray value of the center pixel of the local neighborhood and g_p ($p = 0, \dots, P-1$) correspond to the gray values of P equally

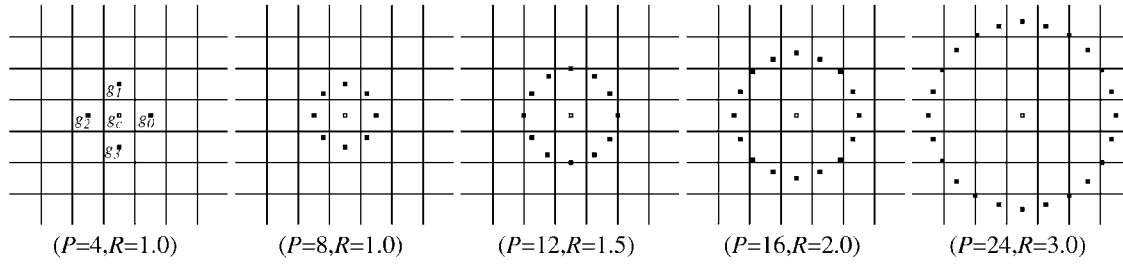


Fig. 1. Circularly symmetric neighbor sets for different (P, R) .

spaced pixels on a circle of radius R ($R > 0$) that form a circularly symmetric neighbor set.

If the coordinates of g_c are $(0, 0)$, then the coordinates of g_p are given by $(-R \sin(2\pi p/P), R \cos(2\pi p/P))$. Fig. 1 illustrates circularly symmetric neighbor sets for various (P, R) . The gray values of neighbors which do not fall exactly in the center of pixels are estimated by interpolation.

2.1 Achieving Gray-Scale Invariance

As the first step toward gray-scale invariance, we subtract, without losing information, the gray value of the center pixel (g_c) from the gray values of the circularly symmetric neighborhood g_p ($p = 0, \dots, P-1$), giving:

$$T = t(g_c, g_0 - g_c, g_1 - g_c, \dots, g_{P-1} - g_c). \quad (2)$$

Next, we assume that differences $g_p - g_c$ are independent of g_c , which allows us to factorize (2):

$$T \approx t(g_c) t(g_0 - g_c, g_1 - g_c, \dots, g_{P-1} - g_c). \quad (3)$$

In practice, an exact independence is not warranted; hence, the factorized distribution is only an approximation of the joint distribution. However, we are willing to accept the possible small loss in information as it allows us to achieve invariance with respect to shifts in gray scale. Namely, the distribution $t(g_c)$ in (3) describes the overall luminance of the image, which is unrelated to local image texture and, consequently, does not provide useful information for texture analysis. Hence, much of the information in the original joint gray level distribution (1) about the textural characteristics is conveyed by the joint difference distribution [28]:

$$T \approx t(g_0 - g_c, g_1 - g_c, \dots, g_{P-1} - g_c). \quad (4)$$

This is a highly discriminative texture operator. It records the occurrences of various patterns in the neighborhood of each pixel in a P -dimensional histogram. For constant regions, the differences are zero in all directions. On a slowly sloped edge, the operator records the highest difference in the gradient direction and zero values along the edge and, for a spot, the differences are high in all directions.

Signed differences $g_p - g_c$ are not affected by changes in mean luminance; hence, the joint difference distribution is invariant against gray-scale shifts. We achieve invariance with respect to the scaling of the gray scale by considering just the signs of the differences instead of their exact values:

$$T \approx t(s(g_0 - g_c), s(g_1 - g_c), \dots, s(g_{P-1} - g_c)), \quad (5)$$

where

$$s(x) = \begin{cases} 1, & x \geq 0 \\ 0, & x < 0. \end{cases} \quad (6)$$

By assigning a binomial factor 2^p for each sign $s(g_p - g_c)$, we transform (5) into a unique $LBP_{P,R}$ number that characterizes the spatial structure of the local image texture:

$$LBP_{P,R} = \sum_{p=0}^{P-1} s(g_p - g_c) 2^p. \quad (7)$$

The name “Local Binary Pattern” reflects the functionality of the operator, i.e., a local neighborhood is thresholded at the gray value of the center pixel into a binary pattern. $LBP_{P,R}$ operator is by definition invariant against any monotonic transformation of the gray scale, i.e., as long as the order of the gray values in the image stays the same, the output of the $LBP_{P,R}$ operator remains constant.

If we set $(P = 8, R = 1)$, we obtain $LBP_{8,1}$, which is similar to the LBP operator we proposed in [27]. The two differences between $LBP_{8,1}$ and LBP are: 1) The pixels in the neighbor set are indexed so that they form a circular chain and 2) the gray values of the diagonal pixels are determined by interpolation. Both modifications are necessary to obtain the circularly symmetric neighbor set, which allows for deriving a rotation invariant version of $LBP_{P,R}$.

2.2 Achieving Rotation Invariance

The $LBP_{P,R}$ operator produces 2^P different output values, corresponding to the 2^P different binary patterns that can be formed by the P pixels in the neighbor set. When the image is rotated, the gray values g_p will correspondingly move along the perimeter of the circle around g_0 . Since g_0 is always assigned to be the gray value of element $(0, R)$ to the right of g_c rotating a particular binary pattern naturally results in a different $LBP_{P,R}$ value. This does not apply to patterns comprising of only 0s (or 1s) which remain constant at all rotation angles. To remove the effect of rotation, i.e., to assign a unique identifier to each rotation invariant local binary pattern we define:

$$LBP_{P,R}^{ri} = \min\{ROR(LBP_{P,R}, i) \mid i = 0, 1, \dots, P-1\}, \quad (8)$$

where $ROR(x, i)$ performs a circular bit-wise right shift on the P -bit number x i times. In terms of image pixels, (8)

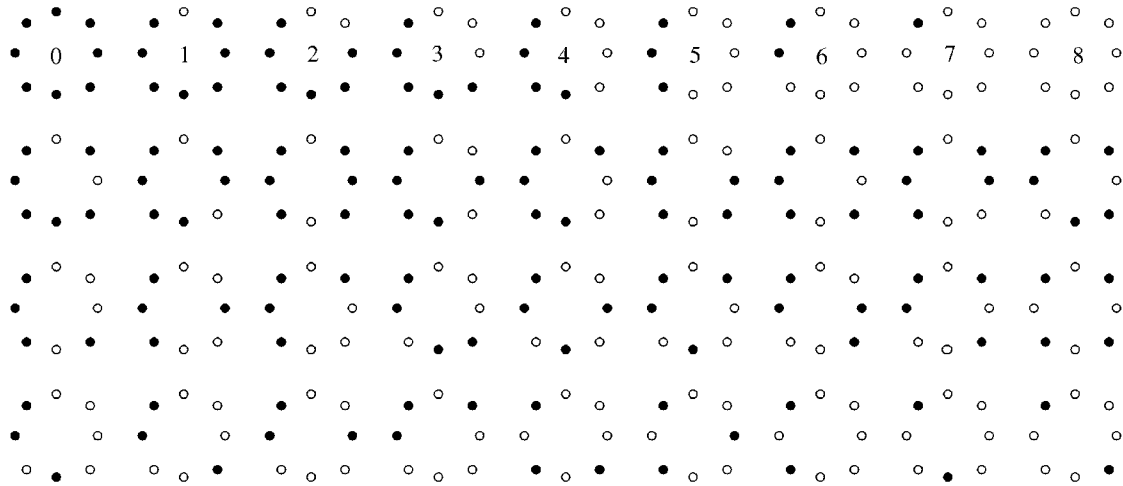


Fig. 2. The 36 unique rotation invariant binary patterns that can occur in the circularly symmetric neighbor set of $LBP_{8,R}^{riu}$. Black and white circles correspond to bit values of 0 and 1 in the 8-bit output of the operator. The first row contains the nine “uniform” patterns and the numbers inside them correspond to their unique $LBP_{8,R}^{riu2}$ codes.

simply corresponds to rotating the neighbor set clockwise so many times that a maximal number of the most significant bits, starting from g_{P-1} , is 0.

$LBP_{P,R}^{riu}$ quantifies the occurrence statistics of individual rotation invariant patterns corresponding to certain micro-features in the image; hence, the patterns can be considered as feature detectors. Fig. 2 illustrates the 36 unique rotation invariant local binary patterns that can occur in the case of $P = 8$, i.e., $LBP_{8,R}^{riu}$ can have 36 different values. For example, pattern #0 detects bright spots, #8 dark spots and flat areas, and #4 edges. If we set $R = 1$, $LBP_{8,1}^{riu}$ corresponds to the gray-scale and rotation invariant operator that we designated as LBP_{ROT} in [29].

2.3 Improved Rotation Invariance with “Uniform” Patterns and Finer Quantization of the Angular Space

Our practical experience, however, has shown that LBP_{ROT} as such does not provide very good discrimination, as we also concluded in [29]. There are two reasons: The occurrence frequencies of the 36 individual patterns incorporated in LBP_{ROT} vary greatly and the crude quantization of the angular space at 45° intervals.

We have observed that certain local binary patterns are fundamental properties of texture, providing the vast majority, sometimes over 90 percent, of all 3×3 patterns present in the observed textures. This is demonstrated in more detail in Section 3 with statistics of the image data used in the experiments. We call these fundamental patterns “uniform” as they have one thing in common, namely, uniform circular structure that contains very few spatial transitions. “Uniform” patterns are illustrated on the first row of Fig. 2. They function as templates for microstructures such as bright spot (0), flat area or dark spot (8), and edges of varying positive and negative curvature (1-7).

To formally define the “uniform” patterns, we introduce a uniformity measure $U(\text{“pattern”})$, which corresponds to the number of spatial transitions (bitwise 0/1 changes) in

the “pattern.” For example, patterns 00000000_2 and 11111111_2 have U value of 0, while the other seven patterns in the first row of Fig. 2 have U value of 2 as there are exactly two 0/1 transitions in the pattern. Similarly, the other 27 patterns have U value of at least 4. We designate patterns that have U value of at most 2 as “uniform” and propose the following operator for gray-scale and rotation invariant texture description instead of $LBP_{P,R}^{riu}$:

$$LBP_{P,R}^{riu2} = \begin{cases} \sum_{p=0}^{P-1} s(g_p - g_c) & \text{if } U(LBP_{P,R}) \leq 2 \\ P+1 & \text{otherwise,} \end{cases} \quad (9)$$

where

$$U(LBP_{P,R}) = |s(g_{P-1} - g_c) - s(g_0 - g_c)| + \sum_{p=1}^{P-1} |s(g_p - g_c) - s(g_{p-1} - g_c)|. \quad (10)$$

Superscript $riu2$ reflects the use of rotation invariant “uniform” patterns that have U value of at most 2. By definition, exactly $P+1$ “uniform” binary patterns can occur in a circularly symmetric neighbor set of P pixels. Equation (9) assigns a unique label to each of them corresponding to the number of “1” bits in the pattern ($0 \leq P$), while the “nonuniform” patterns are grouped under the “miscellaneous” label ($P+1$). In Fig. 2, the labels of the “uniform” patterns are denoted inside the patterns. In practice, the mapping from $LBP_{P,R}$ to $LBP_{P,R}^{riu2}$, which has $P+2$ distinct output values, is best implemented with a lookup table of 2^P elements.

The final texture feature employed in texture analysis is the histogram of the operator outputs (i.e., pattern labels) accumulated over a texture sample. The reason why the histogram of “uniform” patterns provides better discrimination in comparison to the histogram of all individual patterns comes down to differences in their statistical properties. The relative proportion of “nonuniform” patterns of all patterns accumulated into a histogram is so small that their probabilities cannot be estimated reliably.

Inclusion of their noisy estimates in the dissimilarity analysis of sample and model histograms would deteriorate performance.

We noted earlier that the rotation invariance of $LBP_{8,1}^{riu}$ is hampered by the crude 45° quantization of the angular space provided by the neighbor set of eight pixels. A straightforward fix is to use a larger P since the quantization of the angular space is defined by $(360^\circ/P)$. However, certain considerations have to be taken into account in the selection of P . First, P and R are related in the sense that the circular neighborhood corresponding to a given R contains a limited number of pixels (e.g., nine for $R = 1$), which introduces an upper limit to the number of nonredundant sampling points in the neighborhood. Second, an efficient implementation with a lookup table of 2^P elements sets a practical upper limit for P . In this study, we explore P values up to 24, which requires a lookup table of 16 MB that can be easily managed by a modern computer.

2.4 Rotation Invariant Variance Measures of the Contrast of Local Image Texture

The $LBP_{P,R}^{riu2}$ operator is a gray-scale invariant measure, i.e., its output is not affected by any monotonic transformation of the gray scale. It is an excellent measure of the spatial pattern, but it, by definition, discards contrast. If gray-scale invariance is not required and we wanted to incorporate the contrast of local image texture as well, we can measure it with a rotation invariant measure of local variance:

$$VAR_{P,R} = \frac{1}{P} \sum_{p=0}^{P-1} (g_p - \mu)^2, \quad \text{where } \mu = \frac{1}{P} \sum_{p=0}^{P-1} g_p. \quad (11)$$

$VAR_{P,R}$ is by definition invariant against shifts in gray scale. Since $LBP_{P,R}^{riu2}$ and $VAR_{P,R}$ are complementary, their joint distribution $LBP_{P,R}^{riu2}/VAR_{P,R}$ is expected to be a very powerful rotation invariant measure of local image texture. Note that, even though we in this study restrict ourselves to using only joint distributions of $LBP_{P,R}^{riu2}$ and $VAR_{P,R}$ operators that have the same (P, R) values, nothing would prevent us from using joint distributions of operators computed at different neighborhoods.

2.5 Nonparametric Classification Principle

In the classification phase, we evaluate the dissimilarity of sample and model histograms as a test of goodness-of-fit, which is measured with a nonparametric statistical test. By using a nonparametric test, we avoid making any, possibly erroneous, assumptions about the feature distributions. There are many well-known goodness-of-fit statistics such as the chi-square statistic and the G (log-likelihood ratio) statistic [33]. In this study, a test sample S was assigned to the class of the model M that maximized the log-likelihood statistic:

$$L(S, M) = \sum_{b=1}^B S_b \log M_b, \quad (12)$$

where B is the number of bins and S_b and M_b correspond to the sample and model probabilities at bin b , respectively.

Equation (12) is a straightforward simplification of the G (log-likelihood ratio) statistic:

$$G(S, M) = 2 \sum_{b=1}^B S_b \log \frac{S_b}{M_b} = 2 \sum_{b=1}^B [S_b \log S_b - S_b \log M_b], \quad (13)$$

where the first term of the righthand expression can be ignored as a constant for a given S .

L is a nonparametric pseudometric that measures likelihoods that sample S is from alternative texture classes, based on exact probabilities of feature values of preclassified texture models M . In the case of the joint distribution $LBP_{P,R}^{riu2}/VAR_{P,R}$, (12) was extended in a straightforward manner to scan through the two-dimensional histograms.

Sample and model distributions were obtained by scanning the texture samples and prototypes with the chosen operator and dividing the distributions of operator outputs into histograms having a fixed number of B bins. Since $LBP_{P,R}^{riu2}$ has a fixed set of discrete output values ($0 \rightarrow P+1$), no quantization is required, but the operator outputs are directly accumulated into a histogram of $P+2$ bins. Each bin effectively provides an estimate of the probability of encountering the corresponding pattern in the texture sample or prototype. Spatial dependencies between adjacent neighborhoods are inherently incorporated in the histogram because only a small subset of patterns can reside next to a given pattern.

Variance measure $VAR_{P,R}$ has a continuous-valued output; hence, quantization of its feature space is needed. This was done by adding together feature distributions for every single model image in a total distribution, which was divided into B bins having an equal number of entries. Hence, the cut values of the bins of the histograms corresponded to the $(100/B)$ percentile of the combined data. Deriving the cut values from the total distribution and allocating every bin the same amount of the combined data guarantees that the highest resolution of quantization is used where the number of entries is largest and vice versa. The number of bins used in the quantization of the feature space is of some importance as histograms with a too small number of bins fail to provide enough discriminative information about the distributions. On the other hand, since the distributions have a finite number of entries, a too large number of bins may lead to sparse and unstable histograms. As a rule of thumb, statistics literature often proposes that an average number of 10 entries per bin should be sufficient. In the experiments, we set the value of B so that this condition is satisfied.

2.6 Multiresolution Analysis

We have presented general rotation-invariant operators for characterizing the spatial pattern and the contrast of local image texture using a circularly symmetric neighbor set of P pixels placed on a circle of radius R . By altering P and R , we can realize operators for any quantization of the angular space and for any spatial resolution. Multiresolution analysis can be accomplished by combining the information provided by multiple operators of varying (P, R) .

In this study, we perform straightforward multiresolution analysis by defining the aggregate dissimilarity as the

sum of individual log-likelihoods computed from the responses of individual operators

$$L_N = \sum_{n=1}^N L(S^n, M^n), \quad (14)$$

where N is the number of operators and S^n and M^n correspond to the sample and model histograms extracted with operator n ($n = 1, \dots, N$), respectively. This expression is based on the additivity property of the G statistic (13), i.e., the results of several G tests can be summed to yield a meaningful result. If X and Y are independent random events and S_X , S_Y , M_X , and M_Y are the respective marginal distributions for S and M , then $G(S_{XY}, M_{XY}) = G(S_X, M_X) + G(S_Y, M_Y)$ [18].

Generally, the assumption of independence between different texture features does not hold. However, estimation of exact joint probabilities is not feasible due to statistical unreliability and computational complexity of large multidimensional histograms. For example, the joint histogram of $LBP_{8,R}^{riu2}$, $LBP_{16,R}^{riu2}$, and $LBP_{24,R}^{riu2}$ would contain 4,680 ($10 \times 18 \times 26$) cells. To satisfy the rule of thumb for statistical reliability, i.e., at least 10 entries per cell on average, the image should be of roughly $(216 + 2R)(216 + 2R)$ pixels in size. Hence, high-dimensional histograms would only be reliable with really large images, which renders them impractical. Large multidimensional histograms are also computationally expensive, both in terms of computing speed and memory consumption.

We have recently successfully employed this approach also in texture segmentation, where we quantitatively compared different alternatives for combining individual histograms for multiresolution analysis [25]. In this study, we restrict ourselves to combinations of at most three operators.

3 EXPERIMENTS

We demonstrate the performance of our approach with two different problems of rotation invariant texture analysis. Experiment #1 is replicated from a recent study on rotation invariant texture classification by Porter and Canagarajah [31] for the purpose of obtaining comparative results to other methods. Image data includes 16 source textures captured from the Brodatz album [4]. Considering this in conjunction with the fact that rotated textures are generated from the source textures digitally, this image data provides a slightly simplified but highly controlled problem for rotation invariant texture analysis. In addition to the original experimental setup, where training was based on multiple rotation angles, we also consider a more challenging setup, where the texture classifier is trained at only one particular rotation angle and then tested with samples from other rotation angles.

Experiment #2 involves a new set of texture images which have a natural tactile dimension and natural appearance of local intensity distortions caused by the tactile dimension. Some source textures have large intra-class variation in terms of color content, which results in highly different gray-scale properties in the intensity images. Adding the fact that the textures were captured

using three different illuminants of different color spectra, this image data presents a very realistic and challenging problem for illumination and rotation invariant texture analysis.

To incorporate three different spatial resolutions and three different angular resolutions, we realized $LBP_{P,R}^{riu2}$ and $VAR_{P,R}$ with (P, R) values of (8, 1), (16, 2), and (24, 3) in the experiments. Corresponding circularly symmetric neighborhoods are illustrated in Fig. 1. In multiresolution analysis, we use the three 2-resolution combinations and the one 3-resolution combination these three alternatives can form.

Before going into the experiments, we take a quick look at the statistical foundation of $LBP_{P,R}^{riu2}$. In the case of $LBP_{8,R}^{riu2}$, we choose nine “uniform” patterns out of the 36 possible patterns, merging the remaining 27 under the “miscellaneous” label. Similarly, in the case of $LBP_{16,R}^{riu2}$, we consider only 7 percent (17 out of 243) of the possible rotation invariant patterns. Taking into account a minority of the possible patterns and merging a majority of them could imply that we are throwing away most of the pattern information. However, this is not the case, as the “uniform” patterns appear to be fundamental properties of local image texture, as illustrated by the numbers in Table 1.

In the case of the image data of Experiment #1, the nine “uniform” patterns of $LBP_{8,1}^{riu2}$ contribute from 76.6 percent up to 91.8 percent of the total pattern data, averaging 87.2 percent. The most frequent individual pattern is symmetric edge detector 00001111₂ with an 18.0 percent share, followed by 00011111₂ (12.8 percent) and 00000111₂ (11.8 percent); hence, these three patterns contribute 42.6 percent of the textures. As expected, in the case of $LBP_{16,1}^{riu2}$, the 17 “uniform” patterns contribute a smaller proportion of the image data, from 50.9 percent up to 76.4 percent of the total pattern data, averaging 66.9 percent. The most frequent pattern is the flat area/dark spot detector 1111111111111111₂ with an 8.8 percent share.

The numbers for the image data of Experiment #2 are remarkably similar. The contribution of the nine “uniform” patterns of $LBP_{8,1}^{riu2}$ totaled over the three illuminants (see Section 3.2.1) ranges from 82.4 percent to 93.3 percent, averaging 89.7 percent. The three most frequent patterns are again 00001111₂ (18.9 percent), 00000111₂ (15.2 percent), and 00011111₂ (14.5 percent), totalling 48.6 percent of the patterns. The contribution of the 17 “uniform” patterns of $LBP_{16,2}^{riu2}$ ranges from 57.6 percent to 79.6 percent, averaging 70.7 percent. The most frequent patterns is again 1111111111111111₂ with an 8.7 percent share. In the case of $LBP_{24,3}^{riu2}$, the 25 “uniform” patterns contribute 54.0 percent of the local texture. The two most frequent patterns are the flat area/dark spot detector (all bits “1”) with an 8.6 percent share and the bright spot detector (all bits “0”) with an 8.2 percent share.

3.1 Experiment #1

In their comprehensive study, Porter and Canagarajah [31] presented three feature extraction schemes for rotation invariant texture classification, employing the wavelet transform, a circularly symmetric Gabor filter, and a

TABLE 1
Proportions (%) of “Uniform” Patterns of All Patterns for Each Texture
Used in the Experiments and Their Average Over All Textures

Experiment #1				Experiment #2						
Texture				Texture	$P=8, R=1$				$P=16, R=2$	
	$P=8, R=1$	$P=16, R=2$	$P=24, R=3$		‘inca’	‘tl84’	‘horizon’	total	total	total
<i>canvas</i>	84.8	58.5	41.2	<i>canvas001</i>	91.4	90.9	90.4	90.9	71.2	53.4
<i>cloth</i>	91.8	74.2	52.8	<i>canvas002</i>	92.6	91.7	91.1	91.8	73.2	54.2
<i>cotton</i>	88.9	67.0	46.3	<i>canvas003</i>	89.6	89.3	88.2	89.0	68.2	50.4
<i>grass</i>	85.5	63.3	45.6	<i>canvas005</i>	93.5	93.1	93.3	93.3	78.0	61.2
<i>leather</i>	87.7	66.6	49.1	<i>canvas006</i>	87.4	86.4	86.5	86.8	60.8	42.2
<i>matting</i>	89.5	72.0	55.8	<i>canvas009</i>	83.2	82.3	81.9	82.4	59.3	43.8
<i>paper</i>	89.2	70.9	52.9	<i>canvas011</i>	90.6	89.3	89.0	89.6	67.1	48.6
<i>pigskin</i>	87.6	67.9	50.9	<i>canvas021</i>	85.6	85.6	85.4	85.5	57.6	41.0
<i>raffia</i>	91.4	76.4	59.1	<i>canvas022</i>	92.3	91.1	91.0	91.4	78.1	65.0
<i>rattan</i>	86.1	68.5	52.4	<i>canvas023</i>	91.1	90.6	90.2	90.6	69.7	50.9
<i>reptile</i>	88.4	70.9	55.6	<i>canvas025</i>	93.2	92.8	92.7	92.9	76.1	55.0
<i>sand</i>	89.1	70.7	53.4	<i>canvas026</i>	92.2	91.8	91.5	91.8	68.0	47.8
<i>straw</i>	83.8	56.6	40.7	<i>canvas031</i>	93.0	92.5	92.4	92.6	74.3	55.8
<i>weave</i>	76.6	50.9	32.1	<i>canvas032</i>	89.8	88.8	89.4	89.3	66.4	49.0
<i>wood</i>	86.1	65.1	46.1	<i>canvas033</i>	92.8	92.1	91.8	92.2	75.0	56.2
<i>wool</i>	88.9	71.0	55.0	<i>canvas035</i>	90.4	90.1	89.4	90.0	68.4	50.4
AVERAGE	87.2	66.9	49.3	<i>canvas038</i>	91.0	89.7	89.8	90.1	71.4	54.6
				<i>canvas039</i>	92.7	91.7	91.6	92.0	75.8	59.0
				<i>tile005</i>	90.0	89.6	88.3	89.3	71.5	54.3
				<i>tile006</i>	91.0	90.5	89.7	90.4	74.0	57.8
				<i>carpet002</i>	82.8	83.6	81.1	82.5	65.5	55.6
				<i>carpet004</i>	87.6	87.1	86.3	87.0	70.8	57.8
				<i>carpet005</i>	92.2	91.6	91.0	91.6	79.6	67.9
				<i>carpet009</i>	90.8	90.5	89.7	90.3	77.4	64.5
				AVERAGE	90.3	89.7	89.2	89.7	70.7	54.0

Gaussian Markov Random Field with a circularly symmetric neighbor set. They concluded that the wavelet-based approach was the most accurate and exhibited the best noise performance also having the lowest computational complexity.

3.1.1 Image Data and Experimental Setup

The image data included 16 texture classes from the Brodatz album [4] is shown in Fig. 3. For each texture class, there were eight 256×256 source images, of which the first was used for training the classifier, while the other seven images were used to test the classifier. Porter and Canagarajah created 180×180 images of rotated textures from these source images using bilinear interpolation. If the rotation angle was a multiple of 90 degrees (0° or 90° in the case of the present ten rotation angles), a small amount of artificial blur was added to the images to simulate the effect of blurring on rotation at other angles. It should be stressed that the source textures were captured from sheets in the Brodatz album and that the rotated textures were generated digitally from the source images. Consequently, the rotated textures do not have any local intensity distortions such as shadows, which could be caused when a real texture with a natural tactile dimension was rotated with respect to an illuminant and a camera. Thus, this image data provides a slightly simplified but highly controlled problem for rotation invariant texture analysis.

In the original experimental setup, the texture classifier was trained with several 16×16 subimages extracted from the training image. This fairly small size of training samples

increases the difficulty of the problem nicely. The training set comprised rotation angles 0° , 30° , 45° , and 60° , while the textures for classification were presented at rotation angles 20° , 70° , 90° , 120° , 135° , and 150° . Consequently, the test data included 672 samples, 42 (6 angles \times 7 images) for each of the 16 texture classes. Using a Mahalanobis distance classifier, Porter and Canagarajah reported 95.8 percent classification accuracy for the rotation invariant wavelet-based features as the best result.

3.1.2 Experimental Results

We started replicating the original experimental setup by dividing the 180×180 images of the four training angles (0° , 30° , 45° , and 60°) into 121 disjoint 16×16 subimages. In other words, we had 7,744 training samples, 484 (4 angles \times 121 samples) in each of the 16 texture classes. We first computed the histogram of the chosen operator for each of the 16×16 samples. Then, we added the histograms of all samples belonging to a particular class into one big model histogram for this class since the histograms of single 16×16 samples would have been too sparse to be reliable models. Also, using 7,744 different models would have resulted in computational overhead for, in the classification phase, the sample histograms were compared to every model histogram. Consequently, we obtained 16 reliable model histograms containing $484(16 - 2R)^2$ entries (the operators have a R pixel border). The performance of the operators was evaluated with the 672 testing images. Their sample histograms contained $(180 - 2R)^2$ entries; hence, we did not have to worry about their stability.

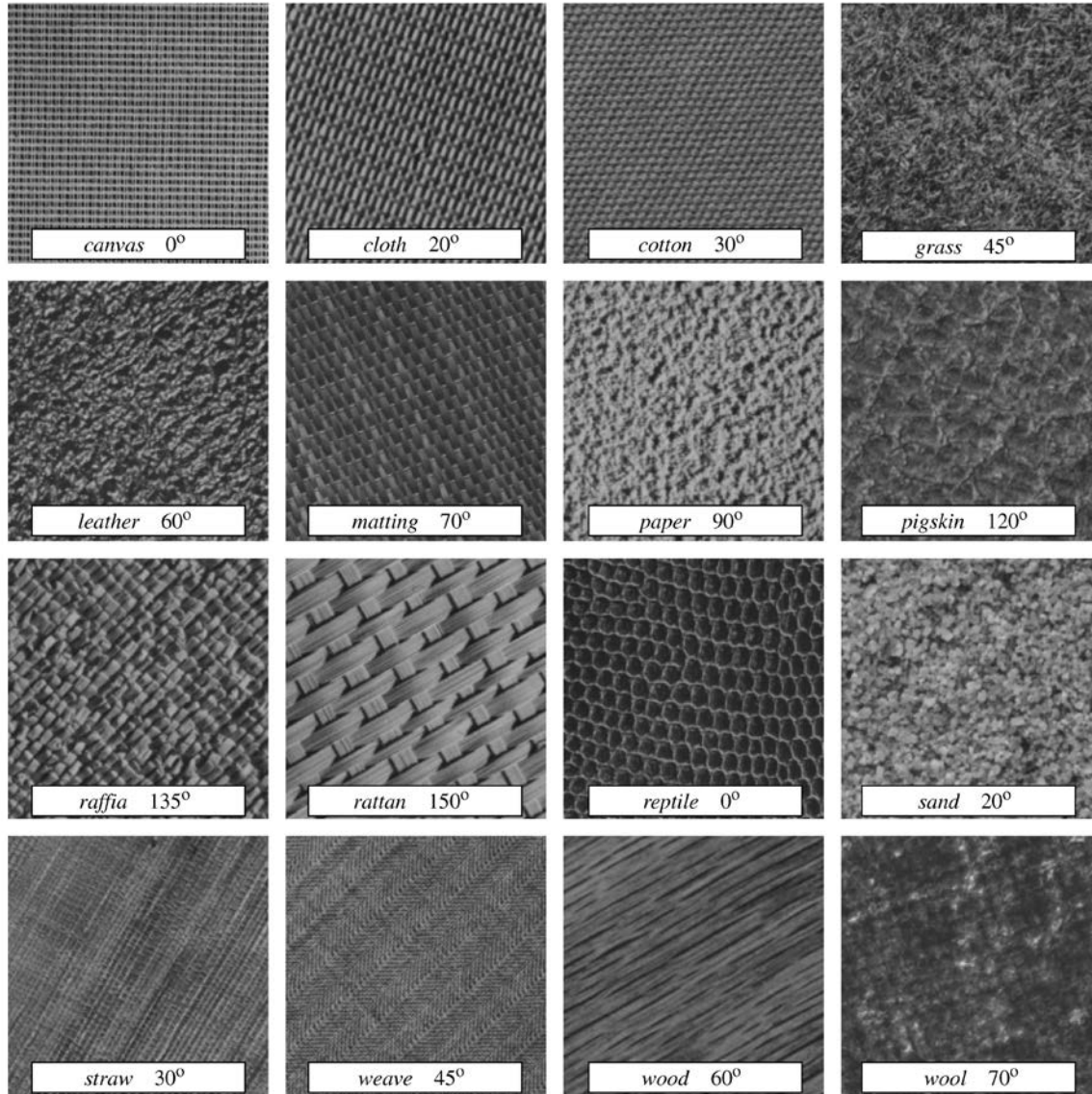


Fig. 3. 180×180 samples of the 16 textures used in Experiment #1 at particular angles.

Results in Table 2 correspond to the percentage of correctly classified samples of all testing samples. As expected, $LBP_{16,2}^{riu2}$ and $LBP_{24,3}^{riu2}$ clearly outperformed their simpler counterpart $LBP_{8,1}^{riu2}$, which had difficulties in discriminating strongly oriented textures, as misclassifications of *rattan*, *straw*, and *wood* contributed 70 of the 79 misclassified samples. Interestingly, in all 79 cases, the model of the true class ranked second, right after the most similar model of a false class that led to misclassification. $LBP_{16,2}^{riu2}$ did much better, classifying all samples correctly except 10 *grass* samples that were assigned to *leather*. Again, in all 10 cases, the model of the true class ranked second. $LBP_{24,3}^{riu2}$ provided further improvement by missing just five *grass* samples and a *matting* sample. In all six cases, the model of the true class again ranked second.

Combining the $LBP_{P,R}^{riu2}$ operator with the $VAR_{P,R}$ operator, which did not do too badly by itself, generally improved the performance. The lone exception was (24, 3),

where the addition of the poorly performing $VAR_{24,3}$ only hampered the excellent discrimination by $LBP_{24,3}^{riu2}$. We see that $LBP_{16,2}^{riu2}/VAR_{16,2}$ fell one sample short of a faultless result as a *straw* sample at 90° angle was labeled as *grass*.

The results for single resolutions are so good that there is not much room for improvement by the multiresolution analysis, though two joint distributions provided a perfect classification. The largest gain was achieved for the $VAR_{P,R}$ operator, especially when $VAR_{24,3}$ was excluded.

Note that we voluntarily discarded the knowledge that training samples come from four different rotation angles, merging all sample histograms into a single model for each texture class. Hence, the final texture model was an “average” of the models of the four training angles, which actually decreased the performance to a certain extent. If we had used four separate models, one for each training angle, for example, $LBP_{16,2}^{riu2}/VAR_{16,2}$ would have provided a perfect classification and the classification error of $LBP_{16,2}^{riu2}$ would have been halved.

TABLE 2

Classification Accuracies (%) for the Original Experimental Setup, where Training Is Done with Rotations 0°, 30°, 45°, and 60°

P,R	$LBP_{P,R}^{riu2}$		$VAR_{P,R}$		$LBP_{P,R}^{riu2}/VAR_{P,R}$	
	BINS	RESULT	BINS	RESULT	BINS	RESULT
8,1	10	88.2	128	95.5	10/16	98.4
16,2	18	98.5	128	88.4	18/16	99.9
24,3	26	99.1	128	86.6	26/16	96.4
8,1+16,2	10+18	99.0	128+128	98.7	10/16+18/16	99.7
8,1+24,3	10+26	99.6	128+128	98.4	10/16+26/16	100.0
16,2+24,3	18+26	99.0	128+128	87.9	18/16+26/16	99.1
8,1+16,2+24,3	10+18+26	99.1	128+128+128	96.6	10/16+18/16+26/16	100.0

Even though a direct comparison to the results of Porter and Canagarajah may not be meaningful due to the different classification principle, the excellent results for our operators demonstrate their suitability for rotation invariant texture classification.

Table 3 presents results for a more challenging experimental setup where the classifier was trained with samples of just one rotation angle and tested with samples of other nine rotation angles. We trained the classifier with the 16×16 samples extracted from the designated training images, again merging the histograms of the 121 16×16 samples of a particular texture class

into one model histogram. The classifier was tested with the samples obtained from the other nine rotation angles of the seven source images reserved for testing purposes, totaling 1,008 samples, 63 in each of the 16 texture classes. Note that the seven testing images in each texture class are physically different from the one designated training image; hence, this setup is a true test for the texture operators' ability to produce a rotation invariant representation of local image texture that also generalizes to physically different samples.

Training with just one rotation angle allows a more conclusive analysis of the rotation invariance of our

TABLE 3

Classification Accuracies (%) when Training Is Done at just One Rotation Angle and the Average Accuracy Over the 10 Angles

OPERATOR	P,R	BINS	TRAINING ANGLE										AVERAGE
			0°	20°	30°	45°	60°	70°	90°	120°	135°	150°	
$LBP_{P,R}^{riu2}$	8,1	10	68.7	86.4	84.7	76.4	85.0	84.3	69.4	84.4	76.3	84.8	80.1
	16,2	18	96.2	99.0	98.6	98.9	98.5	99.1	97.6	98.6	98.7	97.5	98.3
	24,3	26	98.7	98.9	0.9	97.6	99.2	98.2	100	98.7	96.7	98.0	98.5
	8,1+16,2	10+18	94.3	99.5	99.8	99.8	98.5	97.2	92.9	99.6	99.2	99.2	98.0
	8,1+24,3	10+26	96.2	99.6	99.4	98.6	99.4	98.9	97.2	99.5	98.3	99.4	98.7
	16,2+24,3	18+26	97.7	100	99.8	99.2	99.3	100	99.6	99.4	98.5	98.4	99.2
	8,1+16,2+24,3	10+18+26	97.6	100	100	100	100	100	98.5	100	98.6	99.8	99.4
$VAR_{P,R}$	8,1	128	92.7	96.6	94.6	94.0	95.6	96.9	93.9	94.2	94.6	95.6	94.9
	16,2	128	89.9	84.5	86.2	90.5	87.3	85.6	91.0	89.8	90.8	88.5	88.4
	24,3	128	85.4	86.4	85.7	84.4	85.4	85.6	86.0	86.7	86.3	85.9	85.8
	8,1+16,2	128+128	97.5	96.9	98.8	99.0	97.9	97.7	97.5	99.1	98.8	97.9	98.1
	8,1+24,3	128+128	95.2	97.0	98.7	98.9	97.5	98.5	96.1	99.5	99.0	97.9	97.8
	16,2+24,3	128+128	88.3	86.5	86.8	86.9	85.5	86.5	89.3	86.9	87.5	87.1	87.1
	8,1+16,2+24,3	128+128+128	94.9	94.6	97.0	98.3	96.2	96.2	95.0	98.2	98.1	97.3	96.6
$LBP_{P,R}^{riu2}/VAR_{P,R}$	8,1	10/16	99.1	94.2	95.7	97.3	95.2	94.4	99.3	96.0	97.3	95.6	96.4
	16,2	18/16	100	99.5	99.4	99.4	99.4	99.6	100	99.5	99.5	99.7	99.6
	24,3	26/16	95.8	95.0	96.2	97.4	96.0	95.5	95.6	97.2	97.9	97.9	96.5
	8,1+16,2	10/16+18/16	100	99.3	99.1	99.2	99.3	99.2	100	99.3	99.3	99.4	99.4
	8,1+24,3	10/16+26/16	99.8	99.8	99.6	99.8	99.6	99.8	99.6	99.7	99.8	99.9	99.7
	16,2+24,3	18/16+26/16	97.2	98.9	98.9	99.8	99.6	99.9	97.3	99.6	99.8	99.9	99.1
	8,1+16,2+24,3	10/16+18/16+26/16	100	99.7	99.5	99.8	99.6	99.7	99.8	99.6	99.8	99.9	99.7

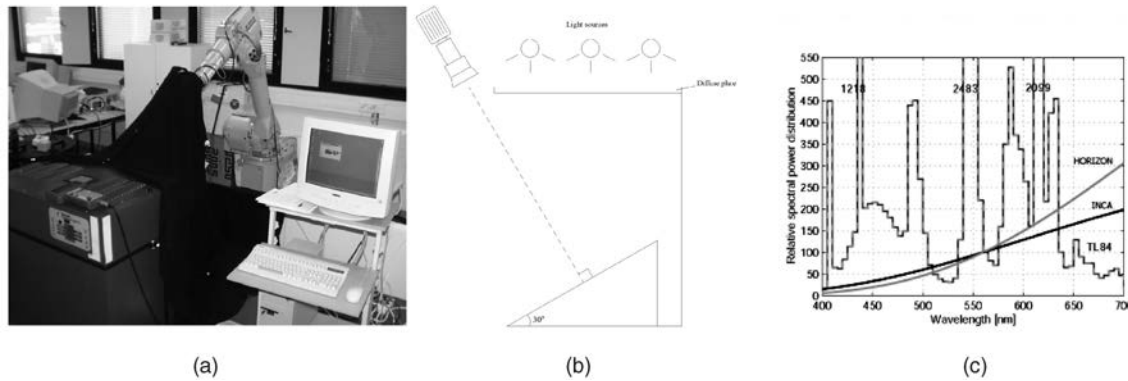


Fig. 4. (a) Imaging setup. (b) Relative positions of texture sample, illuminant, and camera. (c) Spectra of the illuminants.

operators. For example, it is hardly surprising that $LBP_{8,1}^{riu2}$ provides the worst performance when the training angle is a multiple of 45° . Due to the crude quantization of the angular space the presentations learned at 0° , 45° , 90° , or 135° do not generalize that well to other angles.

Again, the importance of the finer quantization of the angular space shows as $LBP_{16,2}^{riu2}$ and $LBP_{24,3}^{riu2}$ provide a solid performance with average classification accuracy of 98.3 percent and 98.5 percent, respectively. In the case of the 173 misclassifications by $LBP_{16,2}^{riu2}$, the model of the true class always ranked second. In the case of the 149 misclassifications by $LBP_{24,3}^{riu2}$, the model of the true class ranked second 117 times and third 32 times.

There is a strong suspicion that the weaker results for $LBP_{16,2}^{riu2}$ at training angles 0° and 90° were due to the artificial blur added to the original images at angles 0° and 90° . The effect of the blur can also be seen in the results of the joint distributions $LBP_{8,1}^{riu2}/VAR_{8,1}$ and $LBP_{16,2}^{riu2}/VAR_{16,2}$, which achieved the best performance when the training angle is either 0° or 90° , the (16, 2) joint operator in fact provides a perfect classification in these cases. Namely, when training was done at some other rotation angle, test angles 0° and 90° contributed most of the misclassified samples, actually all of them in the case of $LBP_{16,2}^{riu2}/VAR_{16,2}$. Nevertheless, the result for $LBP_{16,2}^{riu2}/VAR_{16,2}$ is quite excellent, whereas $LBP_{24,3}^{riu2}/VAR_{24,3}$ seems to suffer from the poor discrimination of the variance measure.

Even though the results for multiresolution analysis generally exhibit improved discrimination over single resolutions, they also serve as a welcome reminder that the addition of inferior operator does not necessarily enhance the performance.

3.2 Experiment #2

3.2.1 Image Data and Experimental Setup

In this experiment, we used textures from Outex, which is a publicly available framework for experimental evaluation of texture analysis algorithms [26]. Outex provides a large collection of textures and ready-made test suites for different types of texture analysis problems, together with baseline results for well-known published algorithms.

The surface textures available in the Outex image database are captured using the setup shown in Fig. 4a. It includes a Macbeth SpectraLight II Luminare light source and a Sony DXC-755P three chip CCD camera attached to

a robot arm. A workstation controls the light source for the purpose of switching on the desired illuminant, the camera for the purpose of selecting desired zoom dictating the spatial resolution, the robot arm for the purpose of rotating the camera into the desired rotation angle and the frame grabber for capturing 24-bit RGB images of size 538 (height) \times 716 (width) pixels. The relative positions of a texture sample, illuminant, and camera are illustrated in Fig. 4b.

Each texture available at the site is captured using three different simulated illuminants provided in the light source: 2300K horizon sunlight denoted as "horizon," 2856K incandescent CIE A denoted as "inca," and 4000K fluorescent tl84 denoted as "tl84." The spectra of the illuminants are shown in Fig. 4c. The camera is calibrated using the "inca" illuminant. It should be noted that, despite the diffuse plate, the imaging geometry is different for each illuminant due to their different physical location in the light source. Each texture is captured using six spatial resolutions (100, 120, 300, 360, 500, and 600 dpi) and nine rotation angles (0° , 5° , 10° , 15° , 30° , 45° , 60° , 75° , and 90°); hence, 162 images are captured from each texture.

The frame grabber produces rectangular pixels whose aspect ratio (height/width) is roughly 1.04. The aspect ratio is corrected by stretching the images in horizontal direction to size 538×746 using Matlab's *imresize* command with bilinear interpolation. Bilinear interpolation is employed instead of bicubic because the latter may introduce halos or extra noise around edges or in areas of high contrast, which would be harmful to texture analysis. Horizontal stretching is used instead of vertical size reduction because sampling images captured by an interline transfer camera along scan lines produces less noise and digital artifacts than sampling across the scan lines.

In this study, we used images captured at the 100 dpi spatial resolution. 24-bit RGB images were transformed into eight bit intensity images using the standard formula:

$$I = 0.299R + 0.587G + 0.114B. \quad (15)$$

Twenty nonoverlapping 128×128 texture samples were extracted from each intensity image by centering the 5×4 sampling grid so that equally many pixels were left over on each side of the sampling grid (13 pixels above and below, 53 pixels left and right). To remove the effect of global first and second order gray-scale properties, which are unrelated

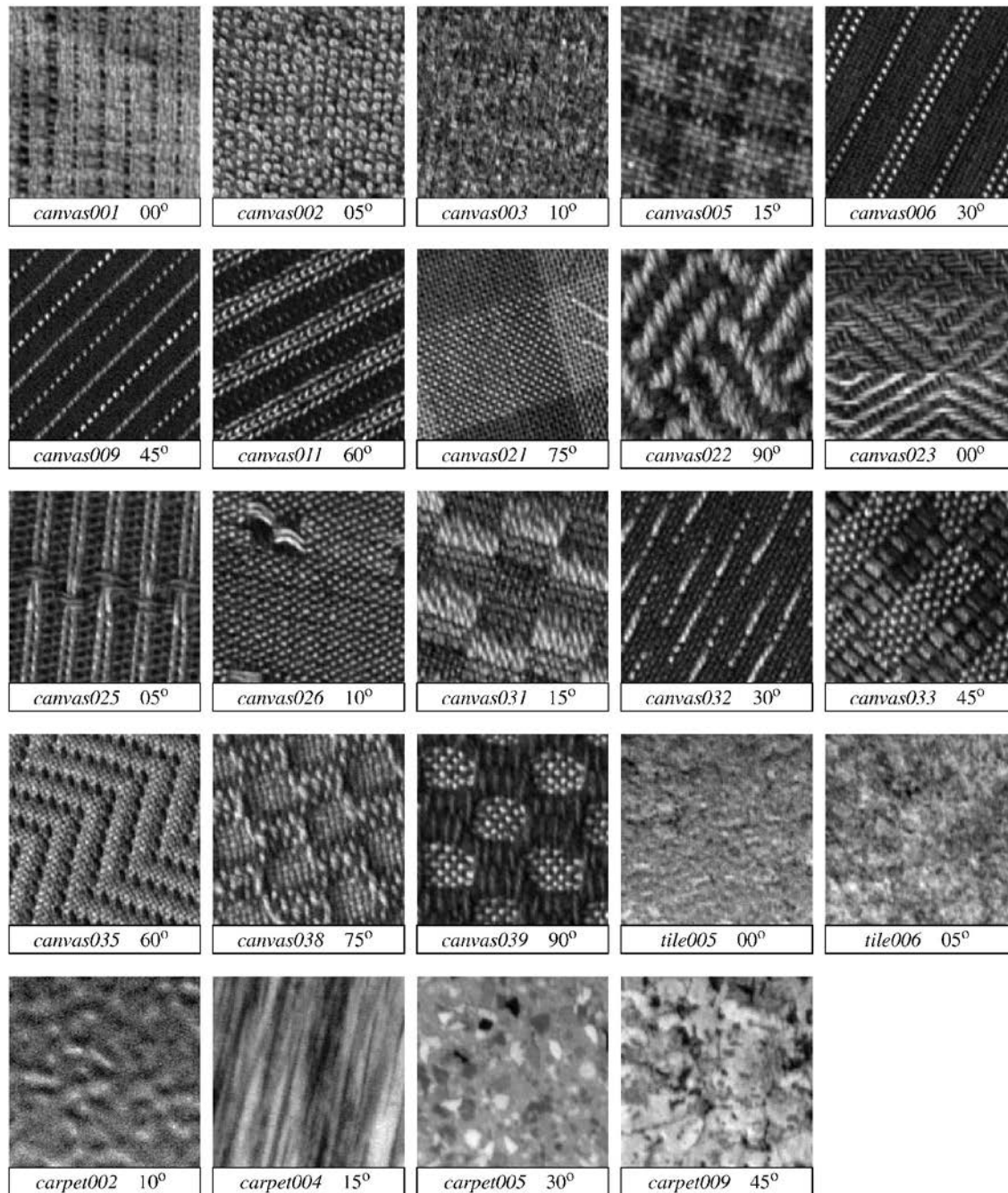


Fig. 5. 128×128 samples of the 24 textures used in Experiment #2 at particular angles.

to local image texture, each 128×128 texture sample was individually normalized to have an average intensity of 128 and a standard deviation of 20. In every forthcoming experiment, the classifier was trained with the samples extracted from images captured using illuminant “inca” and angle 0° (henceforth termed the reference textures).

We selected the 24 textures shown in Fig. 5. While selecting the textures, the underlying texture pattern was required to be roughly uniform over the whole source image, while local gray-scale variations due to varying color properties of the source texture were allowed (e.g., *canvas023* and *canvas033*, shown in Fig. 6). Most of the texture samples are canvases with strong directional

structure. Some of them have a large tactile dimension (e.g., *canvas025*, *canvas033*, and *canvas038*), which can induce considerable local gray-scale distortions. Taking variations caused by different spectra of the illuminants into account, we can conclude that this collection of textures presents a realistic and challenging problem for illumination and rotation invariant texture analysis.

The selection of textures was partly guided by the requirement that the reference textures could be separated from each other. This allowed quantifying our texture operators’ ability to discriminate rotated textures without any bias introduced by the inherent difficulty of the problem. When the 480 samples (24 classes \times 20) were

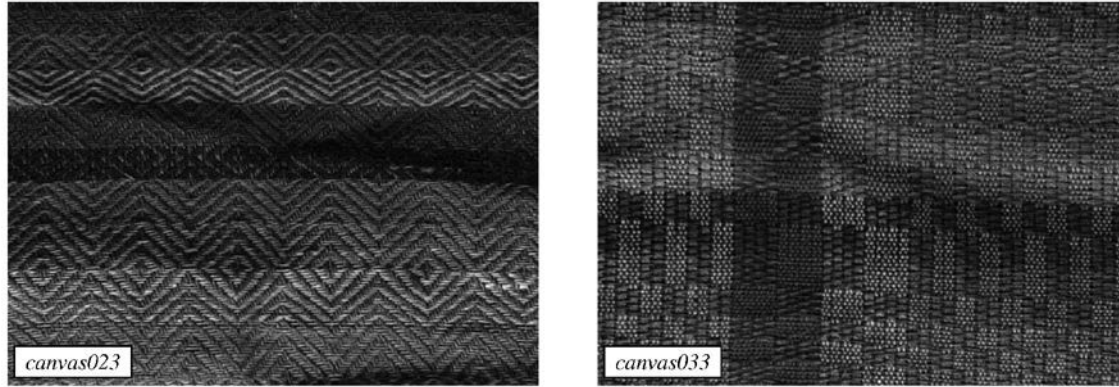


Fig. 6. Intraclass gray-scale variations caused by varying color content of source textures.

randomly halved 100 times so that half of the 20 samples in each texture class served as models for training the classifier and the other 10 samples were used for testing the classifier with the 3-NN method (sample was assigned to the class of the majority of the three most similar models), 99.4 percent average classification accuracy was achieved with the simple rotation variant $LBP_{8,1}^{riu2}$ operator (7). The performance loss incurred by considering just rotation invariant “uniform” patterns is demonstrated by the 93.2 percent average accuracy obtained with the corresponding rotation invariant operator $LBP_{8,1}^{riu2}$. $LBP_{16,2}^{riu2}$ and $LBP_{24,3}^{riu2}$ achieved average classification accuracies of 94.6 percent and 96.3 percent, respectively, in classifying the reference textures.

3.2.2 Results for The Proposed Method

We considered two different setups:

1. **Rotation invariant texture classification (test suite *Outex_TC_00010*):** The classifier is trained with the reference textures (20 samples of illuminant “inca” and angle 0° in each texture class), while the 160 samples of the the same illuminant “inca” but the other eight other rotation angles in each texture class, are used for testing the classifier. Hence, in this suite, there are 480 (24×20) models and 3,840 ($24 \times 20 \times 8$) validation samples in total.
2. **Rotation and illuminant invariant texture classification (test suite *Outex_TC_00012*):** The classifier is trained with the reference textures (20 samples of illuminant “inca” and angle 0° in each texture class) and tested with all samples captured using illuminant “tl84” (problem 000) and “horizon” (problem 001). Hence, in both problems, there are 480 (24×20) models and 4,320 ($24 \times 20 \times 9$) validation samples in total.

In *Outex*, the performance of a texture classification algorithm is characterized with score (S), which corresponds to the percentage of correctly classified samples. Scores for the proposed operators, obtained using the 3-NN method, in rotation invariant texture classification are shown in Table 4. Of individual operators, $LBP_{24,3}^{riu2}$ produced the best score of 94.6 percent which, recalling the 96.3 percent score in the classification of reference textures, demonstrates the robustness of the operator with

respect to rotation. $LBP_{24,3}^{riu2}/VAR_{24,3}$ achieved the best result of joint operators (97.8 percent), which is a considerable improvement over either of the individual operators, underlining their complementary nature. Multiresolution analysis generally improved the performance and the highest score (97.9 percent) was obtained with the combination of $LBP_{8,1}^{riu2}/VAR_{8,1}$ and $LBP_{24,3}^{riu2}/VAR_{24,3}$.

We offer the three employed combinations of (P, R) ((8, 1), (16, 2), and (24, 3)) as a reasonable starting point for realizing the operators, but there is no guarantee that they produce the optimal operator for a given task. For example, when test suite *Outex_TC_00010* was tackled with 189 $LBP_{P,R}^{riu2}$ operators realized using ($P = 4, 5, \dots, 24$; $R = 1.0, 1.5, \dots, 5.0$), the best score of 97.2 percent was obtained with $LBP_{22,4}^{riu2}$. Thirty-two of the 189 operators beat the 94.6 percent score obtained with $LBP_{24,3}^{riu2}$. Fourteen of those 32 operators were realized with ($P = 11 \dots 24$; $R = 4.0$) and they produced the eight highest scores (97.2-97.0 percent). Task or even texture class driven selection of texture operators could be conducted by optimizing cross validation classification of the training data, for example.

Table 5 shows the numbers of misclassified samples for each texture and rotation angle for $LBP_{24,3}^{riu2}$, $VAR_{24,3}$, and $LBP_{24,3}^{riu2}/VAR_{24,3}$, allowing detailed analysis of the discrimination of individual textures and the effect of rotation. $LBP_{24,3}^{riu2}$ classified seven out of the 24 classes completely

TABLE 4
Scores (%) for the Proposed Texture Operators in Rotation Invariant Texture Classification (Test Suite *Outex_TC_00010*)

P, R	$LBP_{P,R}^{riu2}$	$VAR_{P,R}$	$LBP_{P,R}^{riu2}/VAR_{P,R}$
8,1	85.1	91.2	95.4
16,2	88.5	90.7	97.2
24,3	94.6	86.2	97.8
8,1 + 16,2	93.1	93.5	97.4
8,1 + 24,3	96.3	95.2	97.9
16,2 + 24,3	95.4	91.9	97.8
8,1 + 16,2 + 24,3	96.1	94.7	97.7

TABLE 5
The Numbers of Misclassified Samples for Each Texture and Rotation Angle
for $LBP_{24,3}^{riu2}$ (plain), $VAR_{24,3}$ (italic), and $LBP_{24,3}^{riu2}/VAR_{24,3}$ (**bold**) in the Base Problem

Texture	Rotation angle								Total	
	5°	10°	15°	30°	45°	60°	75°	90°		
<i>canvas001</i>	. 3 .	. 4 .	. 5 .	. 5 .	. 2 .	. 2 .	. 6 .	. 10 .	. 37 .	
<i>canvas002</i>	1 1 .	1 1 .	
<i>canvas003</i>	. 1 .	. 1 2 .	. 2 .	. 1 .	. 3 .	. 4 .	. 14 .	
<i>canvas005</i>	1 . .	6 1 .	8 . 2	15 1 2	
<i>canvas011</i>	4	2	6 . .	
<i>canvas021</i>	. 4 .	. 3 .	. 2 .	. 3 .	. 4 .	. 1 .	. 1 .	. 2 .	. 20 .	
<i>canvas023</i>	. 11 .	. 18 .	. 16 .	2 18 2	. 18 1	. 17 1	. 14 .	. 17 .	2 129 4	
<i>canvas025</i>	. 1 .	. 1 .	. 2 .	. 2 1 .	3 . .	3 7 .	
<i>canvas031</i>	. 1 .	. 2 .	. 1 .	. 6 .	1 1 .	3 1 .	6 2 .	11 6 .	21 20 .	
<i>canvas032</i> 1 .	1 1 .	6 5 1	8 5 1	6 5 2	21 17 4	
<i>canvas033</i>	3 6 2	3 8 5	2 10 6	2 12 6	9 13 7	9 8 5	10 10 10	10 11 9	48 78 50	
<i>canvas035</i>	. . .	3 . .	3 1 .	2 1 .	2 1 1	2 . .	2 1 .	1 1 .	15 5 1	
<i>canvas038</i>	. 2 .	. 1 .	. 3 .	2 3 .	4 2 .	6 5 .	9 5 .	9 3 .	30 24 .	
<i>canvas039</i>	1 3 .	1 2 .	1 5 .	2 3 .	2 4 .	2 5 .	5 7 .	6 7 .	20 36 .	
<i>tile005</i>	. 5 .	. 3 1	1 2 2	. 6 1	1 6 2	1 5 1	. 1 1	. 9 3	3 37 11	
<i>tile006</i>	. 6 1	. 5 .	1 5 1	1 7 1	2 5 1	2 8 .	3 5 3	5 6 4	14 47 11	
<i>carpet002</i> 1 .	1 2 .	. 1 .	. 3 .	. 2 .	1 9 .	
<i>carpet004</i>	. 3 .	. 3 2 .	1	1 2 .	. 1 .	2 11 .	
<i>carpet005</i> 1 .	2 . .	2 . .	4 1 .	
<i>carpet009</i>	. 4 .	. 5 1	. 2 1	1 8 .	. 2 .	. 3 .	1 5 .	1 7 .	3 36 2	
$LBP_{24,3}^{riu2}$	4 1.9%	7 3.3%	9 4.3%	12 5.7%	28 13.3%	33 15.7%	55 26.2%	62 29.5%	209 94.6%	
$VAR_{24,3}$	50 9.4%	56 10.6%	54 10.2%	80 15.1%	63 11.9%	63 11.9%	72 13.6%	92 17.4%	530 86.2%	
$LBP_{24,3}^{riu2}/VAR_{24,3}$	3 3.5%	7 8.2%	10 11.8%	10 11.8%	12 14.1%	8 9.4%	15 17.7%	20 23.5%	85 97.8%	

Column total percentage corresponds to the percentage of the column total of all misclassified samples. Only textures with misclassified samples are included.

correctly, having most difficulties with *canvas033* (48/160 misclassified, 19 assigned to *canvas038*, 16 to *canvas031*). $LBP_{24,3}^{riu2}/VAR_{24,3}$ got 16 of the 24 classes correct and well over half of the 2.2 percent error was contributed by 50 misclassified *canvas038* samples. In 20 of the 24 classes, the joint operator did at least as well as either of the

individual operators, demonstrating the usefulness of complementary analysis. However, the four exceptions (*canvas005*, *canvas023*, *canvas033*, *tile005*) remind that joint analysis is not guaranteed to provide the optimal performance. By studying the column totals and the contributions of individual rotation angles to misclassifications, we see

TABLE 6
Scores (%) for the Proposed Operators in Rotation
and Illumination Invariant Texture Classification (Test Suite *Outex_TC_00012*)

P,R	$LBP_{P,R}^{riu2}$		$VAR_{P,R}$		$LBP_{P,R}^{riu2}/VAR_{P,R}$	
	't184'	'horizon'	't184'	'horizon'	't184'	'horizon'
8,1	67.5	62.7	64.3	64.7	78.8	76.7
16,2	81.2	74.1	67.1	72.5	86.1	84.8
24,3	84.0	80.5	62.6	68.9	86.6	87.2
8,1 + 16,2	83.8	78.3	71.5	72.5	85.0	82.6
8,1 + 24,3	90.2	84.1	75.2	76.7	87.2	86.3
16,2 + 24,3	86.4	82.5	71.6	74.6	87.4	87.0
8,1 + 16,2 + 24,3	88.8	83.4	74.9	76.2	87.3	86.4

The classifier is trained with reference textures (illuminant "inca") and tested with samples captured using illuminants "t184" (problem 000) and "horizon" (problem 001).

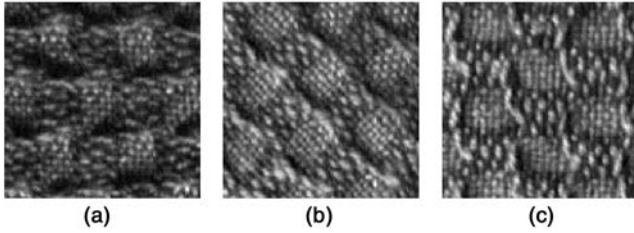


Fig. 7. Three samples of *canvas038*: (a) “inca,” 0° , (b) “horizon,” 45° , and (c) “t184,” 90° .

that each operator had the most misclassifications at high rotation angles. For example, angle 90° contributed almost 30 percent of the misclassified samples in the case of $LBPr_{24,3}^{riu2}$. This attributes to the different image acquisition properties of the interline transfer camera in horizontal and vertical directions.

Scores in Table 6 illustrate the performance in rotation and illumination invariant texture classification. The classifier was trained with the reference textures (“inca,” 0°) and tested with samples captured using a different illuminant. The scores for “horizon” and “t184” include samples from all nine rotation angles, i.e., 180 samples of each texture were used for testing the classifier.

We see that classification performance deteriorated clearly when the classifier was evaluated with samples captured under different illumination than the reference textures used in training. It is difficult to quantify to which extent this is due to the differences in the spectral properties of the illuminants affecting the colors of textures and to which extent due to the different imaging geometries of the illuminants affecting the appearance of local distortions caused by the tactile dimension of textures.

In terms of rotation and illumination invariant classification, *canvas038* was the most difficult texture for $LBPr_{24,3}^{riu2}$ (143/180 “t184” and 178/180 “horizon” samples misclassified) and $LBPr_{24,3}^{riu2}/VAR_{24,3}$ (140/180 “t184” and 102/180 “horizon” sample misclassified). This is easy to understand when looking at three different samples of *canvas038* in Fig. 7, which illustrate the prominent tactile dimension of *canvas038* and the effect it has on local texture structure under different illumination conditions.

3.2.3 Comparative Results for Wavelet-Based Rotation Invariant Features

For comparison purposes, we implemented the wavelet-based rotation invariant features proposed by Porter and Canagarajah, which they concluded to be a favorable approach over Gabor-based and GMRF-based rotation invariant features [31]. We extracted the features using two different image areas, the 16×16 suggested by Porter and Canagarajah and 128×128 . As a classifier, we used the Mahalanobis distance classifier, just like Porter and Canagarajah.

Table 7 shows the scores for the wavelet-based features extracted with image area 128×128 since they provided slightly better performance than the features extracted with image area 16×16 . When these features were employed in classifying the reference textures using 100 random halvings of the samples into training and testing sets, an average classification accuracy of 84.9 percent was obtained.

In the rotation invariant classification, the wavelet-based features achieved score of 80.4 percent, which is clearly lower than the scores obtained with the proposed operators. As demonstrated by the scores for rotation and illumination invariant classification, wavelet-based features appeared to tolerate illumination changes moderately well. Since they are computed over a larger neighborhood, they also characterize macrotextural properties, which are less sensitive to the local changes caused by the different imaging geometries of the illuminants.

Table 7 also shows the percentages of misclassifications contributed by each rotation angle. We observe that 45° contributed the largest number of misclassified samples in all three cases. This is expected for the rotation invariance of wavelet-based features is achieved by averaging horizontal and vertical information by grouping together LH and HL channels in each level of decomposition [31], which results in the weakest estimate in the 45° direction.

In rotation invariant classification, wavelet-based features had the most difficulties in discriminating textures *canvas035* (86/160 samples misclassified), *canvas023* (78/160), *canvas01* (76/160), and *canvas033* (72/160). In rotation and illumination invariant classification, the highest classification errors were obtained for *canvas11* (158/180 “t184” and 163/180 “horizon” samples misclassified).

TABLE 7
Scores (%) for the Wavelet-Based Rotation Invariant Features Proposed
by Porter and Canagarajah and the Percentages of Misclassifications Contributed by Each Rotation Angle

Test suite	Illumination train / test	Score	Rotation angle								
			0°	5°	10°	15°	30°	45°	60°	75°	90°
<i>Outex_TC_00010</i>	‘inca’ / ‘inca’	80.4	-	7.7	6.7	7.9	13.7	22.0	14.3	12.4	15.5
<i>Outex_TC_00012 : 000</i>	‘inca’ / ‘t184’	71.2	8.8	9.3	9.7	9.9	11.6	16.0	12.3	10.6	11.9
<i>Outex_TC_00012 : 001</i>	‘inca’ / ‘horizon’	72.4	10.1	9.0	9.0	9.8	11.8	15.5	12.1	10.9	11.8

4 DISCUSSION

We presented a theoretically and computationally simple yet efficient multiresolution approach to gray-scale and rotation invariant texture classification based on “uniform” local binary patterns and nonparametric discrimination of sample and prototype distributions. “Uniform” patterns were recognized to be a fundamental property of texture as they provide a vast majority of local texture patterns in examined textures, corresponding to texture microstructures such as edges. By estimating the distributions of these microstructures, we combined structural and statistical texture analysis.

We developed a generalized gray-scale and rotation invariant operator $LBP_{P,R}^{riu2}$, which allows for detecting “uniform” patterns in circular neighborhoods of any quantization of the angular space and at any spatial resolution. We also presented a simple method for combining responses of multiple operators for multiresolution analysis by assuming that the operator responses are independent.

Excellent experimental results obtained in two problems of true rotation invariance where the classifier was trained at one particular rotation angle and tested with samples from other rotation angles demonstrate that good discrimination can be achieved with the occurrence statistics of “uniform” rotation invariant local binary patterns.

The proposed approach is very robust in terms of gray-scale variations caused, e.g., by changes in illumination intensity since the $LBP_{P,R}^{riu2}$ operator is by definition invariant against any monotonic transformation of the gray scale. This should make it very attractive in situations where nonuniform illumination conditions are a concern, e.g., in visual inspection. Gray-scale invariance is also necessary if the gray-scale properties of the training and testing data are different. This was clearly demonstrated in our recent study on supervised texture segmentation with the same image set that was used by Randen and Husoy in their recent extensive comparative study [32]. In our experiments, the basic 3×3 LBP operator provided better performance than any of the methods benchmarked by Randen and Husoy for 10 of the 12 texture mosaics and, in most cases, by a clear margin [28]. Results in Experiment #2, involving three illuminants with different spectra and large intraclass color variations in source textures demonstrate that the proposed approach is also robust in terms of color variations.

Computational simplicity is another advantage as the operators can be realized with a few comparisons in a small neighborhood and a lookup table. This facilitates a very straightforward and efficient implementation, which may be mandatory in time critical applications.

If gray-scale invariance is not required, performance can be further improved by combining the $LBP_{P,R}^{riu2}$ operator with the rotation invariant variance measure $VAR_{P,R}$ that characterizes the contrast of local image texture. As we observed in the experiments, the joint distributions of these orthogonal operators are very powerful tools for rotation invariant texture analysis.

The spatial size of the operators is of interest. Some may find our experimental results surprisingly good considering how small spatial support our operators have, for example, in comparison to much larger Gabor filters that are often used in texture analysis. However, the built-in spatial support of our operators is inherently larger as only a limited subset of patterns can reside adjacent to a particular pattern. Still, our operators may not be suitable for discriminating textures where the dominant features appear at a very large scale. This can be addressed by increasing the spatial predicate R , which allows generalizing the operators to any neighborhood size.

The performance can be further enhanced by multiresolution analysis. We presented a straightforward method for combining operators of different spatial resolutions for this purpose. Experimental results involving three different spatial resolutions showed that multiresolution analysis is beneficial, except in those cases where a single resolution was already sufficient for a very good discrimination. Ultimately, we would want to incorporate scale invariance, in addition to gray-scale and rotation invariance.

Regarding future work, one thing deserving a closer look is the use of a task specific subset of rotation invariant patterns, which may, in some cases, provide better performance than “uniform” patterns. Patterns or pattern combinations are evaluated with some criterion, e.g., classification accuracy on a training data, and the combination providing the best accuracy is chosen. Since combinatorial explosion may prevent an exhaustive search through all possible subsets, suboptimal solutions such as stepwise or beam search should be considered. We have explored this approach in a classification problem involving 16 textures from the CURET database [10] with an 11.25° tilt between training and testing images [24]. Thanks to its invariance against monotonic gray-scale transformations, the methodology is applicable to textures with minor 3D transformations, corresponding to such textures which a human can easily, without attention, classify to the same categories as the original textures. Successful discrimination of CURET textures captured from slightly different viewpoints demonstrates the robustness of the approach with respect to small distortions caused by height variations, local shadowing, etc.

In a similar fashion to deriving a task-specific subset of patterns, instead of using a general purpose set of operators, the parameters P and R could be “tuned” for the task in hand or even for each texture class separately. We also reported that when classification errors occur, the model of the true class very often ranks second. This suggests that classification could be carried out in stages by selecting operators which best discriminate among remaining alternatives.

Our findings suggest that complementary information of local spatial patterns and contrast plays an important role in texture discrimination. There are studies on human perception that support this conclusion. For example, Tamura et al. [34] designated coarseness, edge orientation, and contrast as perceptually important textural properties. The LBP histograms provide information of texture orientation and coarseness, while the local gray-scale variance characterizes contrast. Similarly, Beck et al. [3] suggested that texture segmentation of human perception might occur as a result of

differences in the first-order statistics of textural elements and their parts, i.e., in the *LBP* histogram.

APPENDIX

NOTE

Test suites (include images) used in this paper and a Matlab implementation of the proposed method are available at the Outex site (<http://www.outex.oulu.fi>). The original setup of Experiment #1 is available as test suite *Contrib_TC_00000* (single problem) and the revised setup is available as test suite *Contrib_TC_00001* (10 problems corresponding to training with each of the 10 rotation angles in turn). Experiment #2 is available as test suites *Outex_TC_00010* (rotation invariant texture classification, single problem) and *Outex_TC_00012* (rotation and illumination invariant texture classification, two problems).

ACKNOWLEDGMENTS

The authors wish to thank Dr. Nishan Canagarajah and Mr. Paul Hill from the University of Bristol for providing the texture images of Experiment #1. The authors also would like to thank the anonymous referees for their valuable comments. The financial support provided by the Academy of Finland is gratefully acknowledged.

REFERENCES

- [1] O. Alata, C. Cariou, C. Ramananjara, and M. Najim, "Classification of Rotated and Scaled Textures Using HMHV Spectrum Estimation and the Fourier-Mellin Transform," *Proc. IEEE Int'l Conf. Image Processing*, vol. 1, pp. 53-56, 1998.
- [2] H. Arof and F. Deravi, "Circular Neighbourhood and 1-D DFT Features for Texture Classification and Segmentation," *IEE Proc.—Vision, Image, and Signal Processing*, vol. 145, pp. 167-172, 1998.
- [3] J. Beck, S. Prazdny, and A. Rosenfeld, "A Theory of Textural Segmentation," *Human and Machine Vision*, J. Beck, B. Hope, and A. Rosenfeld, eds., Academic, 1983.
- [4] P. Brodatz, *Textures: A Photographic Album for Artists and Designers*. Dover, 1966.
- [5] S. Chang, L.S. Davis, S.M. Dunn, J.O. Eklundh, and A. Rosenfeld, "Texture Discrimination by Projective Invariants," *Pattern Recognition Letters*, vol. 5, pp. 337-342, 1987.
- [6] J.-L. Chen and A. Kundu, "Rotation and Gray Scale Transform Invariant Texture Identification Using Wavelet Decomposition and Hidden Markov Model," *IEEE Trans. Pattern Analysis and Machine Intelligence*, vol. 16, pp. 208-214, 1994.
- [7] D. Chetverikov, "Experiments in the Rotation-Invariant Texture Discrimination Using Anisotropy Features," *Proc. Sixth Int'l Conf. Pattern Recognition*, pp. 1071-1073, 1982.
- [8] D. Chetverikov, "Pattern Regularity as a Visual Key," *Image and Vision Computing*, vol. 18, pp. 975-985, 2000.
- [9] F.S. Cohen, Z. Fan, and M.A. Patel, "Classification of Rotated and Scaled Texture Images Using Gaussian Markov Random Field Models," *IEEE Trans. Pattern Analysis and Machine Intelligence*, vol. 13, pp. 192-202, 1991.
- [10] K. Dana, S. Nayar, B. van Ginneken, and J. Koenderink, "Reflectance and Texture of Real-World Surfaces," *Proc. Int'l Conf. Computer Vision and Pattern Recognition*, pp. 151-157, 1997. <http://www.cs.columbia.edu/CAVE/curet/>.
- [11] L.S. Davis, "Polarograms: A New Tool for Image Texture Analysis," *Pattern Recognition*, vol. 13, pp. 219-223, 1981.
- [12] L.S. Davis, S.A. Johns, and J.K. Aggarwal, "Texture Analysis Using Generalized Cooccurrence Matrices," *IEEE Trans. Pattern Analysis and Machine Intelligence*, vol. 1, pp. 251-259, 1979.
- [13] S.R. Fountain and T.N. Tan, "Efficient Rotation Invariant Texture Features for Content-Based Image Retrieval," *Pattern Recognition*, vol. 31, pp. 1725-1732, 1998.
- [14] H. Greenspan, S. Belongie, R. Goodman, and P. Perona, "Rotation Invariant Texture Recognition Using a Steerable Pyramid," *Proc. 12th Int'l Conf. Pattern Recognition*, vol. 2, pp. 162-167, 1994.
- [15] G.M. Haley and B.S. Manjunath, "Rotation-Invariant Texture Classification Using a Complete Space-Frequency Model," *IEEE Trans. Image Processing*, vol. 8, pp. 255-269, 1999.
- [16] R.L. Kashyap and A. Khotanzad, "A Model-Based Method for Rotation Invariant Texture Classification," *IEEE Trans. Pattern Analysis and Machine Intelligence*, vol. 8, pp. 472-481, 1986.
- [17] R. Kondepudy and G. Healey, "Using Moment Invariants to Analyze 3-D Color Textures," *Proc. IEEE Int'l Conf. Image Processing*, vol. 2, pp. 61-65, 1994.
- [18] S. Kullback, *Information Theory and Statistics*. Dover, 1997.
- [19] W.-K. Lam and C.-K. Li, "Rotated Texture Classification by Improved Iterative Morphological Decomposition," *IEE Proc. Vision, Image, and Signal Processing*, vol. 144, pp. 171-179, 1997.
- [20] M.M. Leung and A.M. Peterson, "Scale and Rotation Invariant Texture Classification," *Proc. 26th Asilomar Conf. Signals, Systems, and Computers*, vol. 1, pp. 461-465, 1992.
- [21] S.V.R. Madiraju and C.C. Liu, "Rotation Invariant Texture Classification Using Covariance," *Proc. Int'l Conf. Image Processing*, vol. 2, pp. 655-659, 1994.
- [22] V. Manian and R. Vasquez, "Scaled and Rotated Texture Classification Using a Class of Basis Functions," *Pattern Recognition*, vol. 31, pp. 1937-1948, 1998.
- [23] J. Mao and A.K. Jain, "Texture Classification and Segmentation Using Multiresolution Simultaneous Autoregressive Models," *Pattern Recognition*, vol. 25, pp. 173-188, 1992.
- [24] T. Mäenpää, T. Ojala, M. Pietikäinen, and M. Soriano, "Robust Texture Classification by Subsets of Local Binary Patterns," *Proc. 15th Int'l Conf. Pattern Recognition*, vol. 3, pp. 947-950, 2000.
- [25] T. Mäenpää, M. Pietikäinen, and T. Ojala, "Texture Classification by Multi-Predicate Local Binary Pattern Operators," *Proc. 15th Int'l Conf. Pattern Recognition*, vol. 3, pp. 951-954, 2000.
- [26] T. Ojala, T. Mäenpää, M. Pietikäinen, J. Viertola, J. Kyllönen, and S. Huovinen, "Outex—A New Framework for Empirical Evaluation of Texture Analysis Algorithms," *Proc. 16th Int'l Conf. Pattern Recognition*, 2002.
- [27] T. Ojala, M. Pietikäinen, and D. Harwood, "A Comparative Study of Texture Measures with Classification Based on Feature Distributions," *Pattern Recognition*, vol. 29, pp. 51-59, 1996.
- [28] T. Ojala, K. Valkealahti, E. Oja, and M. Pietikäinen, "Texture Discrimination with Multi-Dimensional Distributions of Signed Gray Level Differences," *Pattern Recognition*, vol. 34, pp. 727-739, 2001.
- [29] M. Pietikäinen, T. Ojala, and Z. Xu, "Rotation-Invariant Texture Classification Using Feature Distributions," *Pattern Recognition*, vol. 33, pp. 43-52, 2000.
- [30] M. Porat and Y. Zeevi, "Localized Texture Processing in Vision: Analysis and Synthesis in the Gaborian Space," *IEEE Trans. Biomedical Eng.*, vol. 36, pp. 115-129, 1989.
- [31] R. Porter and N. Canagarajah, "Robust Rotation-Invariant Texture Classification: Wavelet, Gabor Filter and GMRF Based Schemes," *IEE Proc. Vision, Image, and Signal Processing*, vol. 144, pp. 180-188, 1997.
- [32] T. Randen and J.H. Husoy, "Filtering for Texture Classification: A Comparative Study," *IEEE Trans. Pattern Analysis and Machine Intelligence*, vol. 21, pp. 291-310, 1999.
- [33] R.R. Sokal and F.J. Rohlf, *Biometry*. W.H. Freeman, 1969.
- [34] H. Tamura, S. Mori, and T. Yamawaki, "Textural Features Corresponding to Visual Perception," *IEEE Trans. Systems, Man, and Cybernetics*, vol. 8, pp. 460-473, 1978.
- [35] T.N. Tan, "Scale and Rotation Invariant Texture Classification," *IEE Colloquium Texture Classification: Theory and Applications* 1994.
- [36] L. Wang and G. Healey, "Using Zernike Moments for the Illumination and Geometry Invariant Classification of Multi-Spectral Texture," *IEEE Trans. Image Processing*, vol. 7, pp. 196-203, 1998.
- [37] W.-R. Wu and S.-C. Wei, "Rotation and Gray-Scale Transform-Invariant Texture Classification Using Spiral Resampling, Sub-band Decomposition and Hidden Markov Model," *IEEE Trans. Image Processing*, vol. 5, pp. 1423-1434, 1996.
- [38] Y. Wu and Y. Yoshida, "An Efficient Method for Rotation and Scaling Invariant Texture Classification," *Proc. IEEE Int'l Conf. Acoustics, Speech, and Signal Processing*, vol. 4, pp. 2519-2522, 1995.

- [39] J. You and H.A. Cohen, "Classification and Segmentation of Rotated and Scaled Textured Images Using Texture 'Tuned' Masks," *Pattern Recognition*, vol. 26, pp. 245-258, 1993.



Timo Ojala received the MSc (with honors) and Dr.Tech. degrees in electrical engineering from the University of Oulu, Finland, in 1992 and 1997, respectively. He is currently an Academy Fellow of the Academy of Finland and the associate director of the MediaTeam Oulu research group at the University of Oulu. His research interests include distributed multimedia and pattern recognition.



Matti Pietikäinen received the doctor of technology degree in electrical engineering from the University of Oulu, Finland, in 1982. In 1981, he established the Machine Vision Group at the University of Oulu. The research results of his group have been widely exploited in industry. Currently, he is a professor of information technology, the scientific director of Infotech Oulu Research Center, and the director of the Machine Vision and Media Processing Unit at the University of Oulu. From 1980 to 1981 and from 1984 to 1985, he visited the Computer Vision Laboratory at the University of Maryland. His research interests are in machine vision and image analysis. His current research focuses on texture analysis, color and face image analysis, and document image analysis. He has authored more than 120 papers in international journals, books, and conference proceedings, and about 85 other publications or reports. He is an associate editor of the *IEEE Transactions on Pattern Analysis and Machine Intelligence* and *Pattern Recognition* journals. He was the guest editor (with L.F. Pau) of a two-part special issue on "Machine Vision for Advanced Production" for the *International Journal of Pattern Recognition and Artificial Intelligence* (also reprinted as a book by World Scientific in 1996). He was also the editor of the book *Texture Analysis in Machine Vision* (World Scientific, 2000) and has served as a reviewer for numerous journals and conferences. He was the president of the Pattern Recognition Society of Finland from 1989 to 1992. Since 1989, he has served as a member of the governing board of the International Association for Pattern Recognition (IAPR) and became a fellow of the IAPR in 1994. He is also a member of IAPR's education committee and served as its chairman in 1997-98. He has also served on committees of several international conferences. He is a senior member of the IEEE and a member of the IEEE Computer Society.



Topi Mäenpää received the MSc degree in electrical engineering from the University of Oulu, Finland, in 1999 (with honors). He is currently working with the Machine Vision and Media Processing Unit and the Department of Electrical Engineering as a postgraduate student of the national Graduate School in Electronics, Telecommunications, and Automation. His research interests include color and texture analysis, visual inspection with efficient texture methods, and robotics.

► For more information on this or any other computing topic, please visit our Digital Library at <http://computer.org/publications/dlib>.